Chapter 9
Reduced-Order Modeling of Loosening of Two Bolted Joints Considering Shock Excitation

William Jordan, Caleb Munger, Kaitlyn Vigil, Keegan J. Moore, Brittany Ouellette, Keith Tschohl, and Sean T. Kelly

Abstract Loosening of bolted joints can significantly alter the dynamics of an assembled structure when subject to operational loading environments, potentially leading to decreased efficiency or structural failure. As such, modeling this behavior is crucial to ensure long-term structural health and safe operation. While existing modeling approaches have been developed that capture the loosening of a single bolted joint, many of these approaches have relied on high-fidelity finite element models or approximate analytical techniques. In either case, these methods can struggle to generalize to structures containing many bolted joints due to underlying method assumptions and/or becoming computationally infeasible. To address these drawbacks, a novel reduced-order model (ROM) capturing the underlying dynamics of bolted-joint loosening was developed by one of the authors and experimentally validated for systems with a single bolted joint considering both axial and transverse shock excitation. This ROM has also been used to theoretically study a system with two serially connected bolted joints. In pursuit of extending this ROM's use for structures with multiple bolted joints, this work sought to expand its experimental validation and empirically study its applicability for a system with two bolted joints undergoing loosening. The system under consideration is a modified box assembly with removable component (mBARC), with both U-channels removed and the rectangular bar connected directly to the box assembly (BA). Initial experimental efforts include roving hammer modal analyses of: 1) the BA alone, and 2) the mBARC varying the preload in both bolted joints of interest. These results are used to inform linear finite element model validation and ROM parameter identification efforts. Next, experiments using high-energy shock excitation are performed to: 1) demonstrate bolt-loosening dynamics, 2) inform ROM application, and 3) compare with phenomena seen in previous studies. Lastly, conclusions regarding the applicability of this ROM to predict the system's dynamics as a function of bolt preload are provided.

Keywords Bolt loosening · Nonlinear dynamics · Reduced-order modeling · Modal testing · Finite element modeling

William Jordan
School of Civil Engineering and Environmental Science, The University of Oklahoma
e-mail: william.d.jordan-1@ou.edu

Caleb Munger
Department of Mechanical Engineering, Rose-Hulman Institute of Technology
e-mail: mungerct@rose-hulman.edu

Kaitlyn Vigil
Department of Mechanical Engineering, The University of New Mexico
e-mail: kvigil85@unm.edu

Keegan J. Moore
Daniel Guggenheim School of Aerospace Engineering, Georgia Institute of Technology
e-mail: kmoore@gatech.edu

Brittany Ouellette · Keith Tschohl · Sean T. Kelly
Los Alamos National Laboratory
e-mail: britt@lanl.gov; ktschohl@lanl.gov; stkelly@lanl.gov

*William Jordan, Caleb Munger, and Kaitlyn Vigil contributed equally to this work.

© The Author(s), under exclusive license to River Publishers 2026

Kristin B. Zimmerman, PhD (eds.), *Nonlinear Structures & Systems, Vol. 1*, Conference Proceedings of the Society for Experimental Mechanics Series, https://doi.org/10.13052/rp-9788743814122

Introduction

Bolted joints are a widely used fastening method in assembled structures due to their ease of use and versatility. However, due to a variety of factors arising from environmental loading experienced by an as-assembled structure, loosening of bolted joints may occur. This loosening can significantly change the structure's dynamics, potentially leading to joint or complete structural failure [1]. This makes accurate modeling and identification of bolted-joint loosening in as-assembled structures paramount to ensure safe operation and structural health over the structure's lifetime. As such, efforts to model and understand bolt-loosening dynamics have increased in recent decades, with applications ranging from playground equipment to aircraft carriers. In particular, developing an accurate *predictive* modeling framework is of interest to preemptively mitigate or prevent structural failures resulting from bolted-joint loosening.

Although bolt loosening can be caused by a variety of factors such as corrosion [2], relative thread sliding [3], stress relaxation [4], and axial loading [5], one primary cause of loosening is transverse excitation perpendicular to the axial bolt orientation [6, 7]. These factors, individually or together, can cause a change in bolt preload, which here is the physical phenomenon used to describe the degree of loosening that has occurred from an initial state.

Current predictive modeling frameworks for bolt loosening often use: 1) analytical approximations, and/or 2) computationally expensive finite element model (FEM) simulations [1, 8]. Analytical methods often require a large number of simplifying assumptions and are limited to (relatively) simple assembly configurations such as single-bolt connections [9]. As greater computing power has become more readily available, the use of detailed, high-fidelity FEMs to model bolt-loosening dynamics has increased [10, 11]. However, these studies require fine meshes, specifically around threads, to sufficiently capture loosening behavior. As a result, using such techniques for FEMs of assembled structures with hundreds or thousands of bolts would make the model prohibitively large, and thus infeasible to use. To address these challenges, reduced-order models (ROMs) seek to bridge the gap between analytical models and high-fidelity FEMs. In particular, often after: 1) identifying computationally, and/or 2) experimentally determining bolt-loosening parameters, ROMs seek to simulate the dynamics of bolted-joint loosening with the accuracy of FEMs but at the speed of analytical models [12]. Here, the ROM developed by Moore [13] is considered, which approximates a bolted joint as a single nonlinear time-dependent spring with stiffness that is a function of bolt torque or preload.

To empirically study bolt-loosening dynamics, many experimental setups have been developed that: 1) relate bolt preload as a function of torque, 2) explore bolt-loosening regimes under varying excitations (e.g., impact/shock or harmonic), and/or 3) study time-varying bolt stiffness based on modal testing [1, 9, 14]. This work primarily focuses on the last point to use the ROM developed by Moore in [13] for a high-energy shock excitation. Even for systems with a single bolted connection, an equivalent time-varying bolt stiffness can be difficult to predict across the lifespan of a bolt as different types of excitations and environments can additively contribute to cause bolt loosening [13]. This difficulty is further confounded for structures with multiple bolted joints as such structures can exhibit nonlinear, time-dependent responses that result from dynamic interactions between multiple joints [1].

Given the range of dynamics observed theoretically in previous work [1] and unlike previous experimental efforts applying the ROM developed by Moore [13] (which considered a single bolt), this work sought to: 1) extend this ROM's applicability to a structure with multiple bolted joints, and 2) empirically explore the effects of varying bolt preload and the degree of bolt loosening when considering two bolted connections and shock excitation. Similar to the system presented in [1], for the structure considered here which is a fixed-base modified box assembly with removable component (mBARC), a single component (i.e., the bridge or rectangular bar) serves as the primary source of coupling between the attachment locations on the box assembly (BA) (i.e., the blades). Working toward these goals, first, roving hammer modal testing with low-energy impacts was performed for the BA alone to inform initial BA-alone FEM validation efforts, in particular to characterize the fixed-base boundary condition (BC). Next, the bridge was added and a series of mBARC-specific modal tests was performed still considering low-energy impacts. From these tests, the natural frequencies of the mBARC were extracted as the preload was increased for two bolts of interest. These data were used for mBARC FEM validation efforts, with these efforts now primarily focusing on identifying parameters associated with the bolted connections between the bridge and blades. Following these modal tests, a series of high-energy impacts for shock excitation analyses was performed. For all high-energy impacts, along with measuring preload change in time, the wavelet transform (WT) of measured accelerometer response data was used to qualitatively assess the (transient) nonlinearity of the system's dynamics by demonstrating how the system's natural frequencies change as a function of time. To ensure: 1) no loosening occurred during modal testing, 2) preload loss resulting from the considered range of shock excitations was localized to bolts of interest, and 3) sufficient test repeatability, load washers were added on all bolted connections, including those associated with the fixed-base BC. Based on what were found to be necessary requirements to validate the mBARC FEM accounting for preload changes, results and discussion concerning the ROM's applicability are presented.

Methods

Initially, an FEM and ROM were created and validated for the BA alone to provide model confidence by ensuring: 1) alignment with experimental results from BA-alone modal testing, and 2) the bolted fixed-base BC was correctly modeled. The ROM at this stage consisted of developing a reduced-order representation of the BA using Craig-Chang component mode synthesis (CC-CMS). After completing model validation of the full-order and reduced-order systems of the BA alone, the bridge was added along with bushing elements to create the mBARC FEM, with the bushing elements representing the bolted connections between the blades and bridge. This FEM was then validated against experimental natural frequencies extracted from roving hammer modal testing of the mBARC for varying preload conditions with bolt preloads varied symmetrically. Nonlinearities were discovered as the bolt preloads were increased, manifesting as changes in the contact area between the blades and bridge. Thus, dedicated analyses studying the effect of contact area around bridge-to-blade bolted connections within the mBARC FEM were conducted and are discussed in the Results and Discussion section. Shock testing was then performed for a range of high-energy impact excitations in a specific location and direction of interest. Lastly, based on modeling and experimental results, the applicability of the ROM of interest (here, that developed by Moore in [13]) and effects of preload loss/variation were determined and conclusions made. Figure 1 shows a flowchart of these steps.

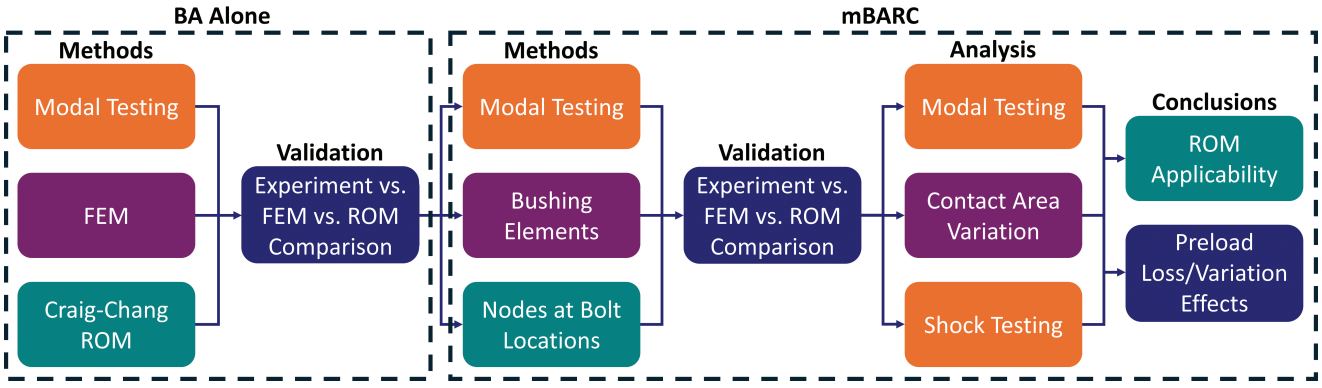

Fig. 1 Testing and analysis flowchart consisting of experimental (), FEM (), ROM (), and additional () steps

Experimental Apparatus

BA and mBARC Setup

The nominal BA of the experimental apparatus is composed of a six-inch side length by three-inch depth by quarter-inch wall thickness square hollow section of aluminum 6061 stock. There is a half-inch wide cutout removing the entire depth of the wall centered along one of the side lengths creating cantilevers on the left and right side of the structure, referred to here as the left and right blades, respectively. For this work, the BA is bolted to an optical breadboard using four 1/4-20 inch fasteners. Adding the rectangular bar (i.e., the bridge), which is also manufactured from aluminum 6061, to the BA completes the mBARC setup and introduces coupling across the (nominally) symmetric blades. Figure 2 shows the experimental setup of the BA alone, and Fig. 3 shows the assembled mBARC. Note that the bridge is bolted to the BA using 10-32 fasteners through the center holes in the group of five holes on each blade (one fastener per blade).

It was found that the BA is sensitive to even minor asymmetries in the fixed-base BC, resulting in large natural frequency differences between the two blades (e.g., experimentally, $>10\%$ difference was achievable in the first natural frequency of each blade). To mitigate the effects of any asymmetry, washers (not shown) were added between the base of the BA/mBARC and the optical breadboard to ensure a constant contact area and BC confidence. The addition of these washers significantly reduced the frequency differences between the blades, and this setup was used to validate the bolted connections at the base of the BA-alone FEM before modeling the mBARC.

Roving Hammer Modal Testing

Initial roving hammer modal testing was conducted on the BA alone to characterize the structure before the bridge was installed and to validate the fixed-base BC in the BA-alone FEM. All impact locations and directions used for this modal testing are shown in Fig. 4. This set of locations and directions remained consistent for both BA-alone and mBARC modal testing. When possible, impact excitations along the global X, Y, and Z axes at each location were considered. However,

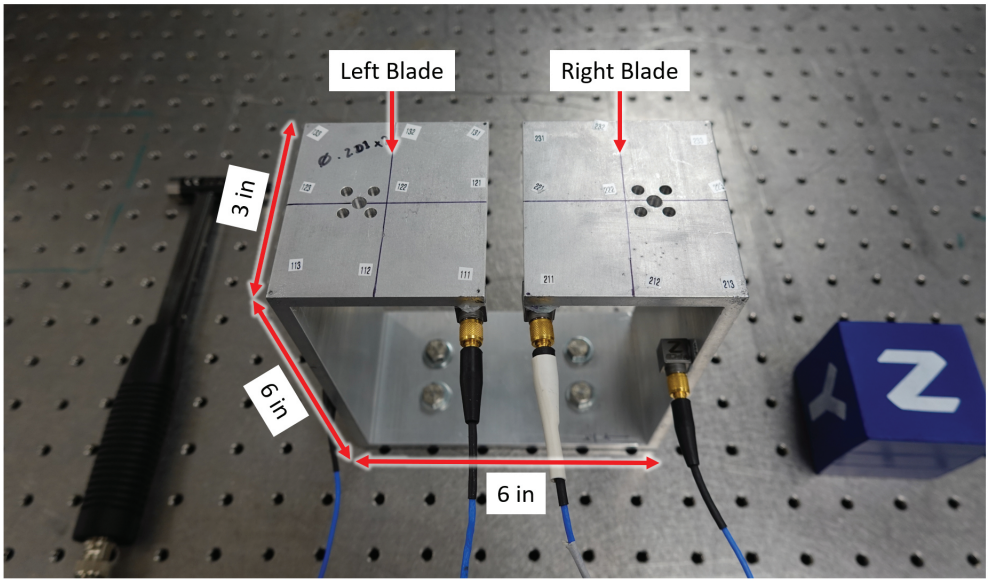

Fig. 2 Front view of the BA alone with all triaxial accelerometers applied

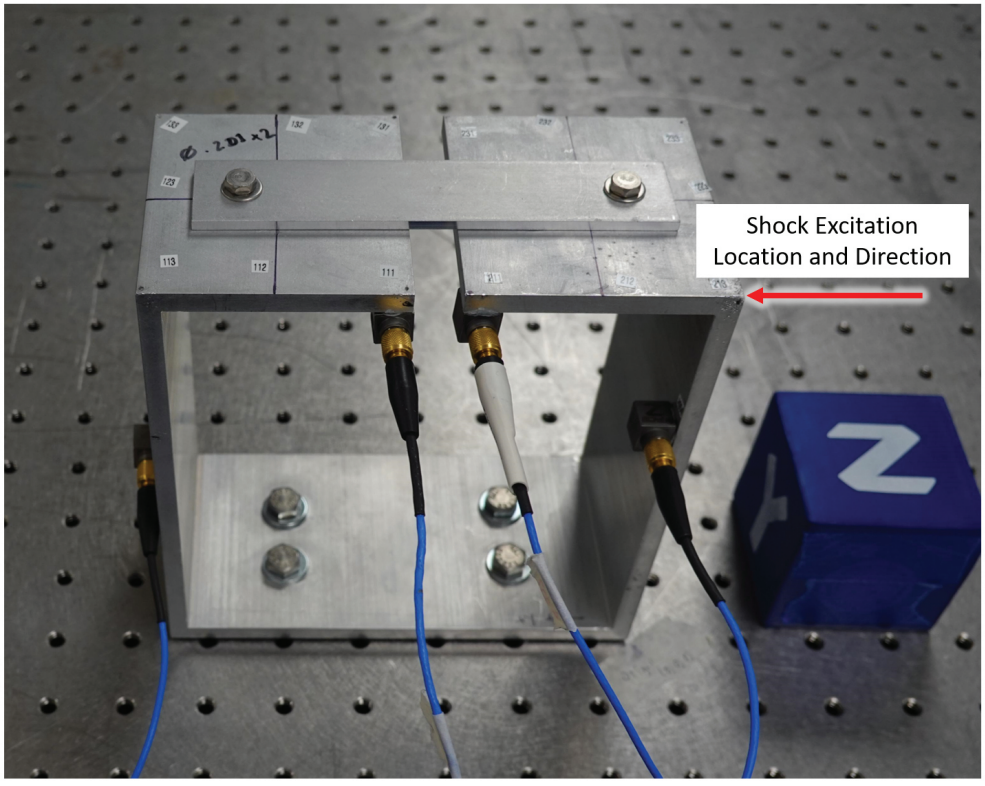

Fig. 3 Front view of the mBARC with all triaxial accelerometers applied. Shock excitation location and direction indicated

several locations could only be excited along one or two axes due to physical constraints of the hammer and/or not having access to a given excitation direction. In total, there were 12 impact locations with (collectively) 28 impact directions.

Multiple types of modal hammers and modal tips were experimented with to determine the hammer-tip combination that produced the cleanest signal. Due to the (relatively) high frequency content and response amplitudes of the BA, the blade edges would respond much quicker than was physically possible to withdraw the hammer during testing, making it challenging to avoid multiple impacts. To resolve this issue, a custom tip was created for the PCB 086C01 impact hammer

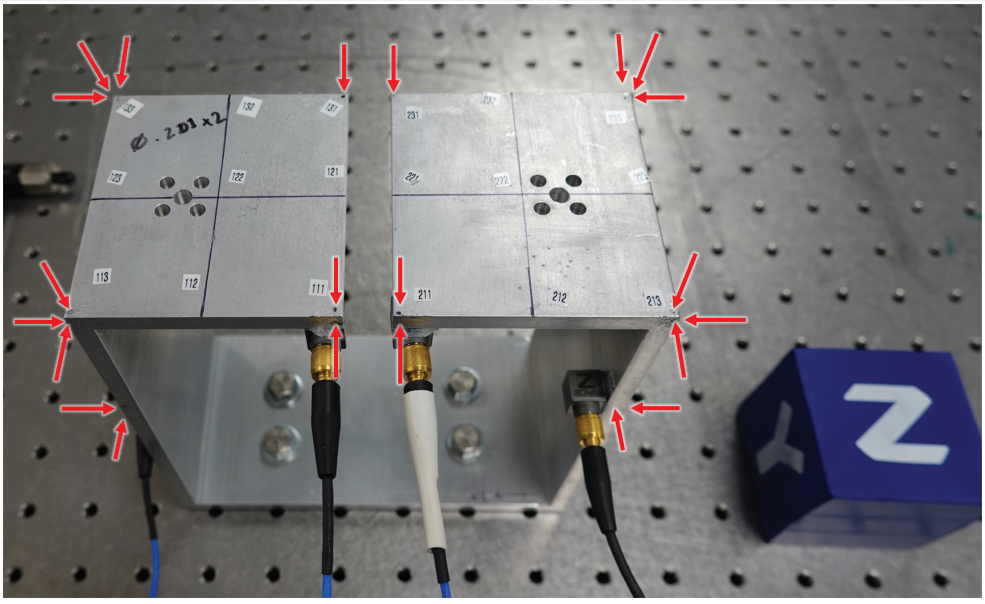

Fig. 4 BA and mBARC roving hammer modal testing impact locations and directions. Two locations and six directions are hidden in the view shown. All impact locations and directions are symmetric about the X-Z midplane

from a set screw and vinyl cap as shown in Fig. 5. This tip expedited BA-alone modal testing by reducing double impacts that often resulted from using harder tips. The PCB 086C03 impact hammer with the PCB 084B04 white, medium nylon tip (no vinyl cap) was sufficient to conduct modal testing on the mBARC and excite higher frequencies without double impacts as the bridge adds structural rigidity. The custom modal tip had a 10 dB roll-off at approximately 600 Hz, and the PCB 084B04 medium nylon tip had a 10 dB roll-off at approximately 1500 Hz. The frequency range of 0–600 Hz contains the first four symmetric modes (i.e., mode pairs) of the BA, and was deemed sufficient for initial BA-alone FEM validation. For the mBARC, the first six system modes were of interest, all of which whose natural frequencies lie below 800 Hz. Thus, the medium nylon tip was used and deemed sufficient.



Fig. 5 Custom modal hammer tip exploded and assembled view

Shock Excitation Testing

During shock excitation testing, the mBARC was impacted at the top right corner in the +Y direction as shown in Fig. 3. For all presented analyses, the bridge-to-blade bolts and their respective load washers to measure preload are labeled F1 and F2, where F2 is closest to the shock, and F1 is furthest from the shock. Figure 6 shows these bolts and their respective load washers on the mBARC. In addition, load washers were added to the four bolts connecting the mBARC to the optical breadboard. The preloads of these bolts were held constant at approximately 7000 N and monitored to ensure they did not loosen during both modal and shock testing. Throughout all testing, the four bolts at the base never loosened.

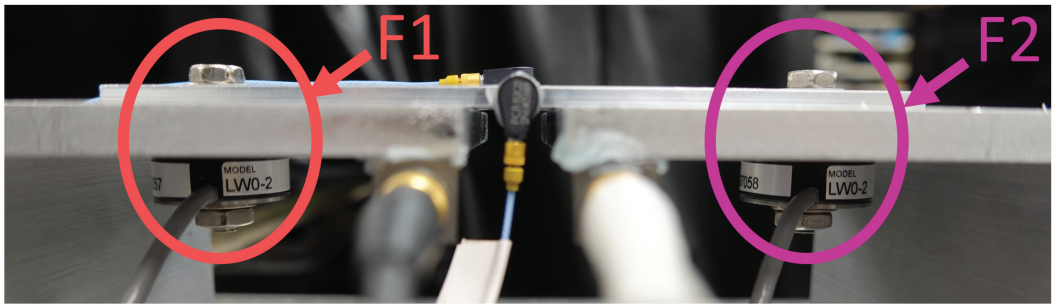

Fig. 6 Close-up view of the bridge on the mBARC with bolts F1 and F2 indicated

Modeling Methods

Finite Element Model

An FEM was iteratively developed to match the experimental apparatus and to be used with the ROM presented in [13]. Figure 7 shows the FEM of the mBARC used in this work (mesh not shown for image clarity). Abaqus/CAE 2024 software was used for all FEM development and analyses. The full mBARC FEM consisted of 33,156 quadratic hexahedral elements (type C3D20R) and 169,721 nodes.

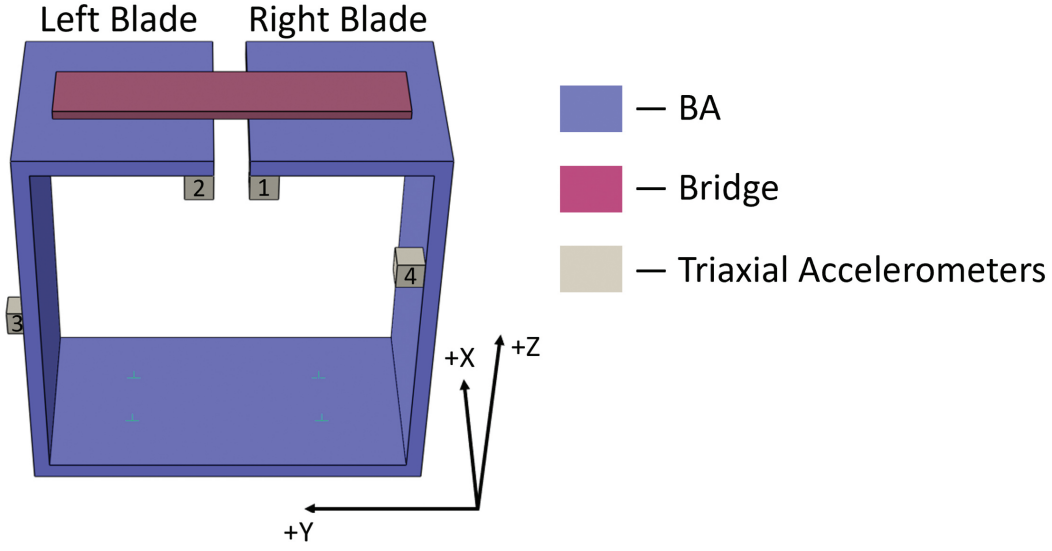

Fig. 7 Front view of the mBARC FEM assembly (mesh not shown for image clarity) with all triaxial accelerometers applied. In practice, all accelerometers were modeled as point masses

Fasteners and bushing elements were used to match experimental and FEM BCs. Specifically, fasteners were used for the fixed-base BC, where the fastener models the clamped volume approximation of the region of influence of a bolted joint [15]. The fastener constraint in Abaqus/CAE creates a specified continuum coupling region and encastres the nodes in the region to the center, which is similar to the clamped volume approximation [15]. Because the natural frequencies of the BA-alone FEM were sensitive to the size of the fastener constraints' continuum coupling regions, this size was changed until the BA-alone FEM sufficiently matched BA-alone experimental results. The experimental and final BA-alone FEM natural frequencies are shown in Table 1.

A six degree-of-freedom (DOF) bushing element was used between the bridge and each of the blades at the F1 and F2 bolt locations to model each bolt. The bushing element has an axial X, Y, and Z stiffness and rotational X, Y, and Z stiffness that can be independently varied when validating the mBARC FEM against experimental natural frequencies. However, as will be discussed, constraints that either: 1) are physically motivated, and/or 2) leverage empirical sensitivities will be added to these axial and rotational stiffness values to reduce the search space for model validation. Figure 8 shows where in the

FEM the bushing element was placed for the left blade (a similar element was added for the right blade) and how the bushing element DOFs are defined.

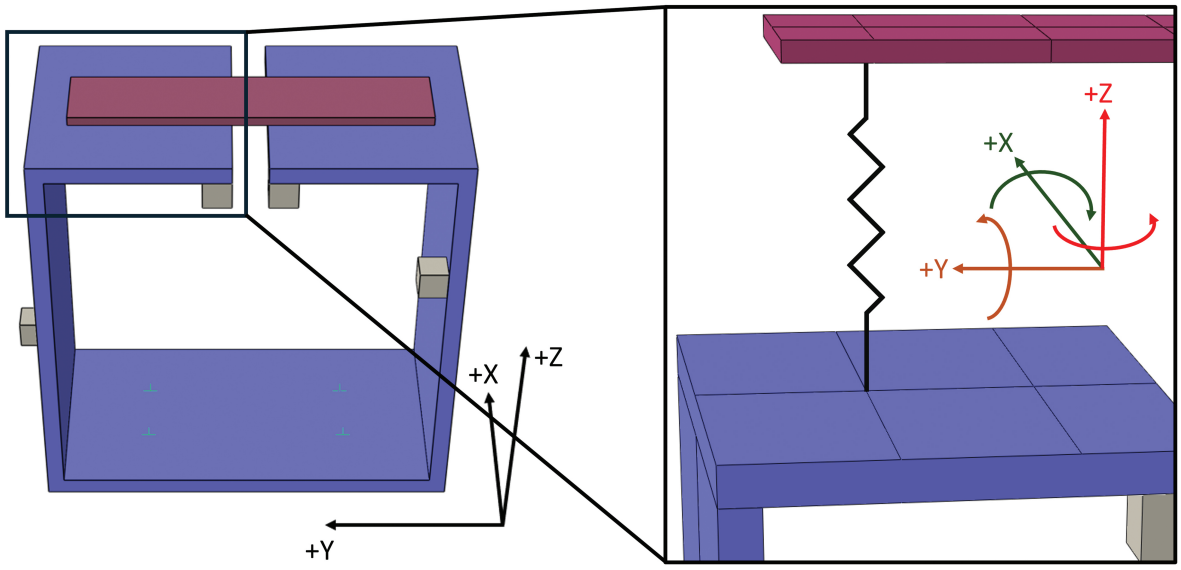

Fig. 8 Visualization of the bushing element in the mBARC FEM for the left blade, which has 3 axial DOFs and 3 rotational DOFs

In addition to changing the stiffness values of the bushing elements, the influence radius of the continuum coupling where each bushing element connects to the bridge and respective blade was changed. Changing the influence radius is an analog to changing the contact area in the experimental setup. Figure 9 shows an example of how the influence radius is specified, with all nodes within the influence radius (i.e., the participating nodes) coupled with a continuum coupling constraint.

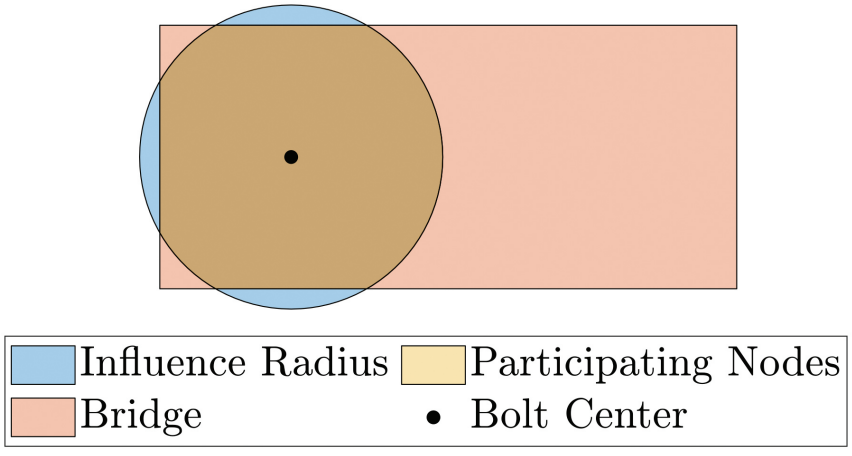

Fig. 9 Example influence radius of a bushing element. The participating nodes are coupled with a continuum coupling constraint, distributing the force over the area defined by the participating nodes

The bushing elements' stiffness values and contact areas were chosen as tunable model parameters as they can be related to physical attributes that could be changed in the experimental mBARC setup. For example, the stiffness could be changed by tightening bolts F1 and F2, and the contact area could be changed due to either bowing of the bridge or the addition of washers between the blades and bridge (discussed further in the Results and Discussion section). As shown in the ROM Applicability section, allowing the contact area and Z rotational stiffness of each bushing element to change was crucial to match experimental results.

Reduced-Order Model

The fundamental idea of the ROM introduced in [13] is that a bolted joint can be modeled as a spring with stiffness $k(T)$ that depends on the instantaneous bolt torque T (here, to be replaced with tension/preload). This model is given in Eq. 1 as:

$$k(T) = k_a \left[1 - \left(1 - \left(\frac{T}{T_m}\right)^{\alpha}\right)^{\beta}\right], \tag{1}$$

where k_a is the maximum possible stiffness, T_m is the theoretical maximum tension/preload, and α and β are dimensionless fitting parameters.

Note that torque was the metric previously used when this ROM was first developed. However, this model was transitioned in [16] to be based on tension. In addition, though the term preload is used throughout this paper, this is similar to the tension metric used in the version of this ROM in [16], and is thus used interchangeably here. Identification of the parameters $k_a = k(T_m)$, α, and β for a single bolt includes three steps. The first step involves conducting modal analyses of the structure at varying bolt preload values. Next, for a given preload, the stiffness of the bolted-joint connection is adjusted in the FEM to align with experimental natural frequencies. This process is repeated for various preloads to produce stiffness-tension (or stiffness-preload) pairs. Lastly, a curve-fitting procedure is then applied using Eq. 1 to identify α and β. k_a and T_m are estimated based on the point where increasing the torque (here, preload) no longer changes the system natural frequencies as this indicates the maximum possible stiffness achievable by the bolted connection has been reached.

This ROM was initially developed for a threaded joint of a split-Hopkinson pressure bar, where the ROM was shown to accurately model the dominant effects of bolt loosening on the dynamic response [13]. Because the impact force and threaded joint were aligned with the longitudinal axis of the bar, the stiffness $k(T)$ of the threaded joint acted only along the longitudinal axis. Therefore, torque only needed to be related to the stiffness along one direction. For the structure considered here, however, the stiffness of bolts F1 and F2 acts in multiple directions. This called for expansion of the ROM to consider multi-direction effects that influence loosening where 1:1 stiffness-torque (or stiffness-tension) pairs are not as readily applicable. In addition, it is important to note this ROM assumes all loosening behavior can be captured by varying stiffness values alone. For brevity, only a summary of this ROM is provided here; however, a comprehensive overview is provided in [13].

Model Validation

As discussed in the Roving Hammer Modal Testing section, the first model validation step was matching the fixed-base BC of the BA alone to the experimental setup. To do so, the bridge was removed from the FEM (Fig. 7, but without the bridge) to reduce model complexity and match the setup shown in Fig. 2. For the BA alone, the natural frequencies of the FEM ($f_{n,FEM}$) have good agreement with the experimental natural frequencies ($f_{n,Exp}$), with all FEM natural frequencies being within 3% for the first eight system modes (i.e., the first four mode pairs resulting from inherent system symmetry). Table 1 shows a comparison of the BA-alone FEM and experimental natural frequencies, with the highest absolute percent error being 2.85% for mode 6.

Table 1 BA-alone FEM and experimental natural frequencies, and absolute percent error in natural frequencies from FEM to experiment

Mode	$f_{n,FEM}$ [Hz]	$f_{n,Exp}$ [Hz]	Absolute % Error
1	98.983	100.23	1.24
2	99.680	100.57	0.88
3	205.13	204.45	0.33
4	206.20	205.45	0.37
5	439.88	429.17	2.50
6	**442.36**	**430.12**	**2.85**
7	478.38	483.67	1.09
8	484.55	475.20	1.97

After validating the fixed-base BC, the bridge was added to the FEM and sensitivity studies conducted using WAVES [17], a Python-based tool that interfaces with Abaqus/CAE and allows for the automation of parametric studies. The Z rotational stiffness and the X and Y axial stiffness values of the bushing elements were varied to study how those stiffness values impacted the mBARC FEM natural frequencies. It was assumed the bolts were symmetric, so the bushing elements were made symmetric (i.e., respective stiffness values in each bushing element were assumed equal). In addition, the X and

Y rotational stiffness values and Z axial stiffness value were held constant at 10^8 N-m/rad and 10^8 N/m, respectively, to prevent the bridge and blades from phasing through each other and mitigate non-physical contact phenomena. These values were chosen by estimating the aluminum 6061 material stiffness when subjected to a deformation/penetration load, though ultimately the modes of interest had little to no sensitivity with respect to these values when sufficiently high to mitigate non-physical contact. The X and Y axial stiffness values were also always assumed equal, as they represent orthogonal tangential directions on the contact surface. Figure 10 shows surface plots of the natural frequencies of modes 1 and 2 as these stiffness values are changed. As shown, the natural frequencies of modes 1 and 2 change by less than 5% over the searched region. This lack of sensitivity is important when fitting the model to experiment, since if the first two natural frequencies lie outside the ranges spanned in Fig. 10, then other model parameters not associated with the bushing element stiffness values need to modified (e.g., see the Contact Area Variability section).

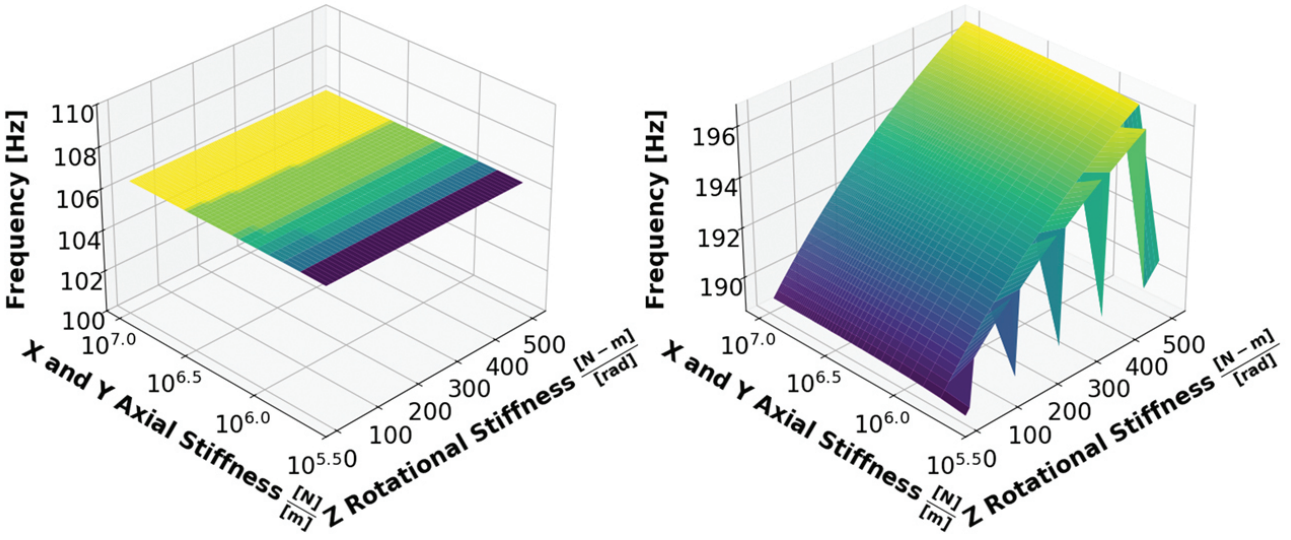

Fig. 10 Natural frequency of (left) mode 1 and (right) mode 2 as the X and Y axial and Z rotational stiffness values are varied. Both frequencies change by less than 5% over the searched region

Similarly, Fig. 11 shows the natural frequencies of modes 4 and 5 as a function of these stiffness values. As shown, the natural frequencies rapidly increase and then plateau as the X and Y axial stiffness values are increased, with minimal

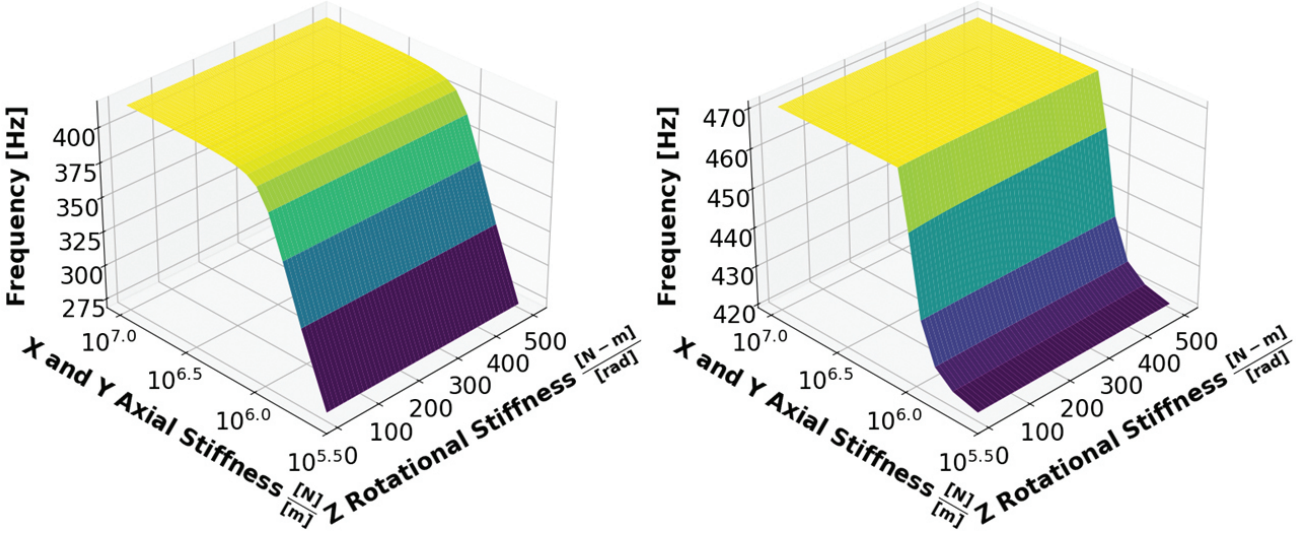

Fig. 11 Natural frequency of (left) mode 4 and (right) mode 5 as the X and Y axial and Z rotational stiffness values are varied. Both frequencies stop changing when the X and Y axial stiffness values are above $10^{6.5}$ N/m

changes resulting from variation in the Z rotational stiffness. Thus, it is clear modes 4 and 5 are almost entirely dictated by the X and Y axial stiffness values.

Figure 12 shows how the natural frequency of mode 3 changes as these stiffness values change. As shown, the natural frequency steadily increases as the Z rotational stiffness is increased, and has little sensitivity with respect to the X and Y axial stiffness values except for low values near $10^{5.5}$ N/m.

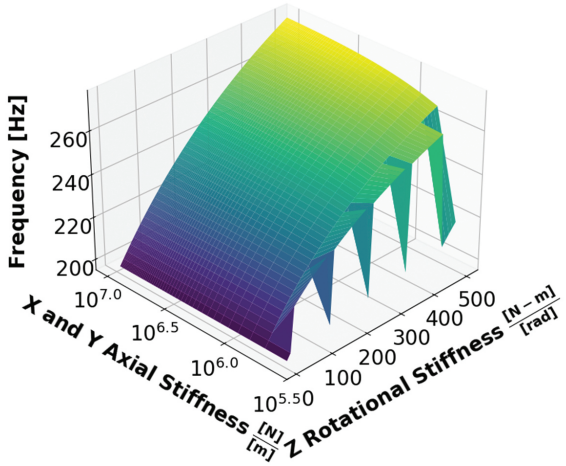

Fig. 12 Natural frequency of mode 3 as the X and Y axial and Z rotational stiffness values are varied. The frequency is primarily dictated by the Z rotational stiffness

The surface plots in Figs. 10–12 were used to tune the mBARC FEM, specifically to determine bushing element stiffness values for different preload values as required for the ROM discussed in the Reduced-Order Model section.

The last parameter in the mBARC FEM that was tuned was the bushing element influence radius. As discussed in the Finite Element Model section, the influence radius controls the simulated contact area between the bridge and each blade. Figure 13 shows how the mBARC FEM natural frequencies for modes 1–6 change as the normalized contact area is varied. A normalized value of 1 means the entire overlapping surface area of the bridge and corresponding blade is in full contact,

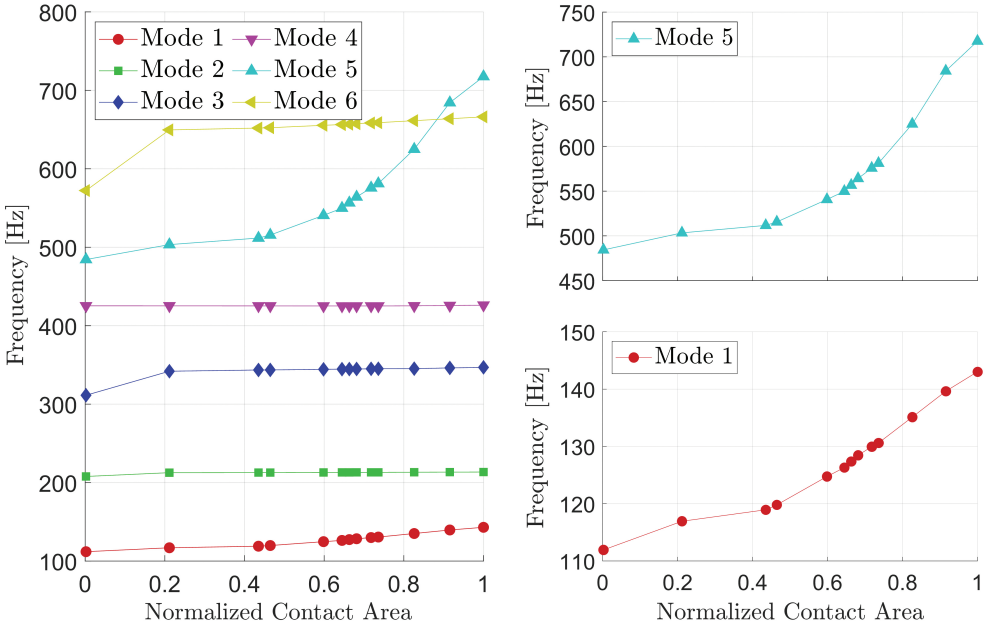

Fig. 13 (left) mBARC FEM natural frequencies for modes 1–6 as the bushing element normalized contact area is changed, with zoomed-in plots of (top right) mode 5 and (bottom right) mode 1. Modes 1 and 5 are most impacted by the changing contact area

with all nodes at the interfaces (as illustrated in Fig. 9) constrained by the bushing element. Conversely, a normalized value of 0 means the bridge and blade are not in contact at all.

As will be shown, changing the contact area was required to match the experimental natural frequencies across the range of preloads considered, as it was found that modifications to bushing element stiffness values alone were insufficient, even considering the range of values shown in Figs. 10–12. Further discussion regarding this requirement is provided in the Contact Area Variability section.

Results and Discussion

The results from this study are presented as follows. First, experimental modal analysis results for the mBARC varying the preload in bolts F1 and F2 are presented. Next, the variation of the contact area between the bridge and blades in the experimental mBARC and FEM is discussed, specifically motivating why such variability explains – and in the FEM was necessary to match – experimental trends. This is followed by results considering high-energy shock excitation to induce bolt loosening. Lastly, a discussion regarding the applicability of the proposed ROM for the mBARC system is provided.

mBARC Modal Analyses

To characterize the interface stiffness between the bridge and blades of the mBARC, separate roving hammer modal tests of the mBARC were performed as the preload in bolts F1 and F2 was simultaneously changed from 200 N to 3000 N. Figure 14 shows the experimental natural frequencies for modes 1–6 at each preload value considered in this range.

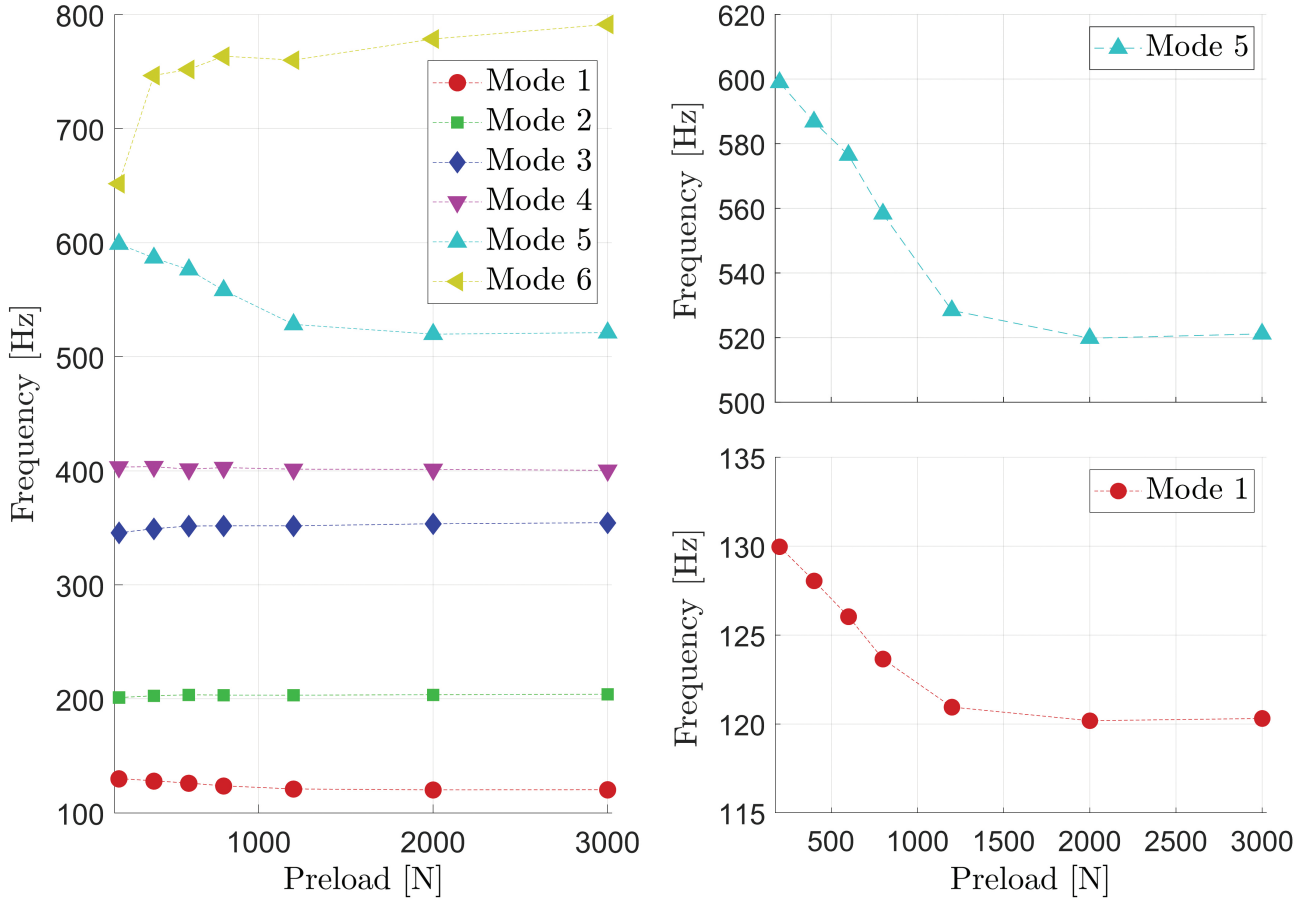

Fig. 14 (left) Experimental mBARC natural frequencies for modes 1–6 as the preload in bolts F1 and F2 was varied from 200 N to 3000 N. Zoomed-in plots of (top right) mode 5 and (bottom right) mode 1. The frequencies of modes 1 and 5 decrease as the preload increases

As shown in Fig. 14, as the preload is increased, the natural frequencies of modes 1 and 5 decrease. Though one may typically expect natural frequencies to increase if not remain constant as preload is increased, after further investigation, it was found that this discrepancy is because the contact area between the bridge and the blades was changing as the preload increased. This was due to bowing of the bridge, thereby decreasing the contact area. As shown in Fig. 13, as the contact area is increased, the natural frequencies of modes 1 and 5 increase, supporting the hypothesis that as the preload is increasing the contact area is decreasing in the experimental mBARC.

Contact Area Variability

To experimentally test the hypothesis that the contact area between the bridge and the blades was changing with preload, a washer was placed between the bridge and each blade of the mBARC for bolts F1 and F2. These added washers are shown in Fig. 15.

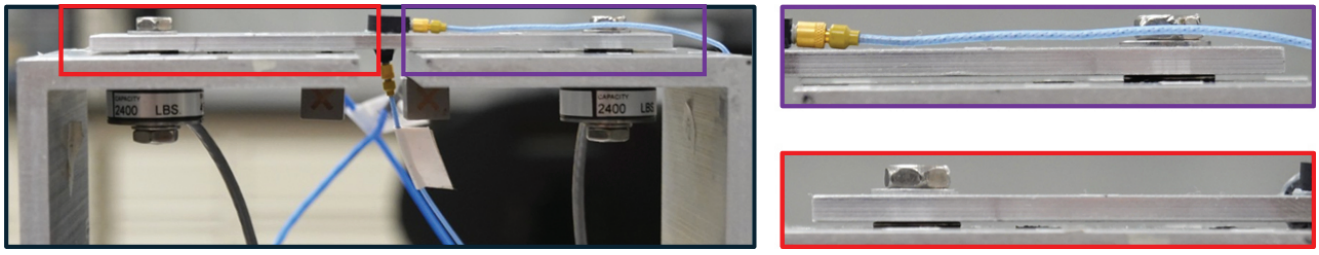

Fig. 15 (left) mBARC experimental setup with a washer added between the bridge and (top right) right and (bottom right) left blades to prevent the contact area from changing with varying preload

Adding a washer between the bridge and each blade ensures a more deterministic, constant contact area such that at all preload values the contact area remains the same. Modal analyses of the mBARC were then performed again for each considered preload to determine the new natural frequencies, which are shown in Fig. 16 overlaid with the natural frequencies from Fig. 14.

Figure 16 demonstrates the effect of adding the washers on the natural frequencies of modes 1–6, and in particular, modes 1, 5, and 6. Regarding mode 6 specifically, when analyzing the measured frequency response functions (FRFs) of the mBARC at preload values less than 1200 N, mode 6 appeared significantly more damped instead of having a sharp peak as was observed for other modes. In addition, for an 800 N preload, there were two heavily damped peaks in the 650–750 Hz frequency range with the corresponding deflection shapes at these peaks not providing sufficient distinction as to which most closely resembled mode 6 at higher bolt preloads. This is why two different natural frequencies are shown in Figs. 16 and 17 for mode 6 at an 800 N preload. Figure 17 shows the natural frequency for mode 6 specifically as the preload in bolts F1 and F2 is varied. Figure 18 shows the natural frequencies of modes 1 and 5 as the preload is varied with and without including washers between the bridge and blades.

From Fig. 18, fixing the contact area between the bridge and each blade results in the natural frequencies of modes 1 and 5 only increasing with increasing preload, as one may more typically expect. This further provides evidence that when not including washers between the bridge and blades, the bridge is bowing and the contact area is decreasing as the preload increases. This is an important conclusion because the ROM discussed in the Reduced-Order Model section neglects the effects of changes in contact area due to changes in preload, and assumes that FEM natural frequencies can sufficiently match experimental natural frequencies (for modes of interest) at each individual preload by varying spring stiffness(es) alone. If the contact area changes in such a way that this cannot be achieved, this ROM cannot be directly used to predict system dynamics during a shock event resulting in bolt loosening. Thus, this ROM was not applicable for the as-manufactured mBARC considered here (without added washers), as varying the contact area was critical and necessary to validate the mBARC FEM against experiment at each preload. This is shown explicitly in the ROM Applicability section. Note that this also rendered the CC-CMS ROM formulation for the BA-alone unusable as well (though good agreement with experiment was achieved; results not shown for brevity), as this would have been used in conjunction with the bolt-loosening ROM to more efficiently perform shock simulations.

After the completion of all experimental modal analyses of the mBARC with washers added between the bridge and the blades, these added washers were removed prior to shock testing because the mBARC as shown in Fig. 3 was ultimately of greatest interest due to using a more common bolted joint assembly configuration.

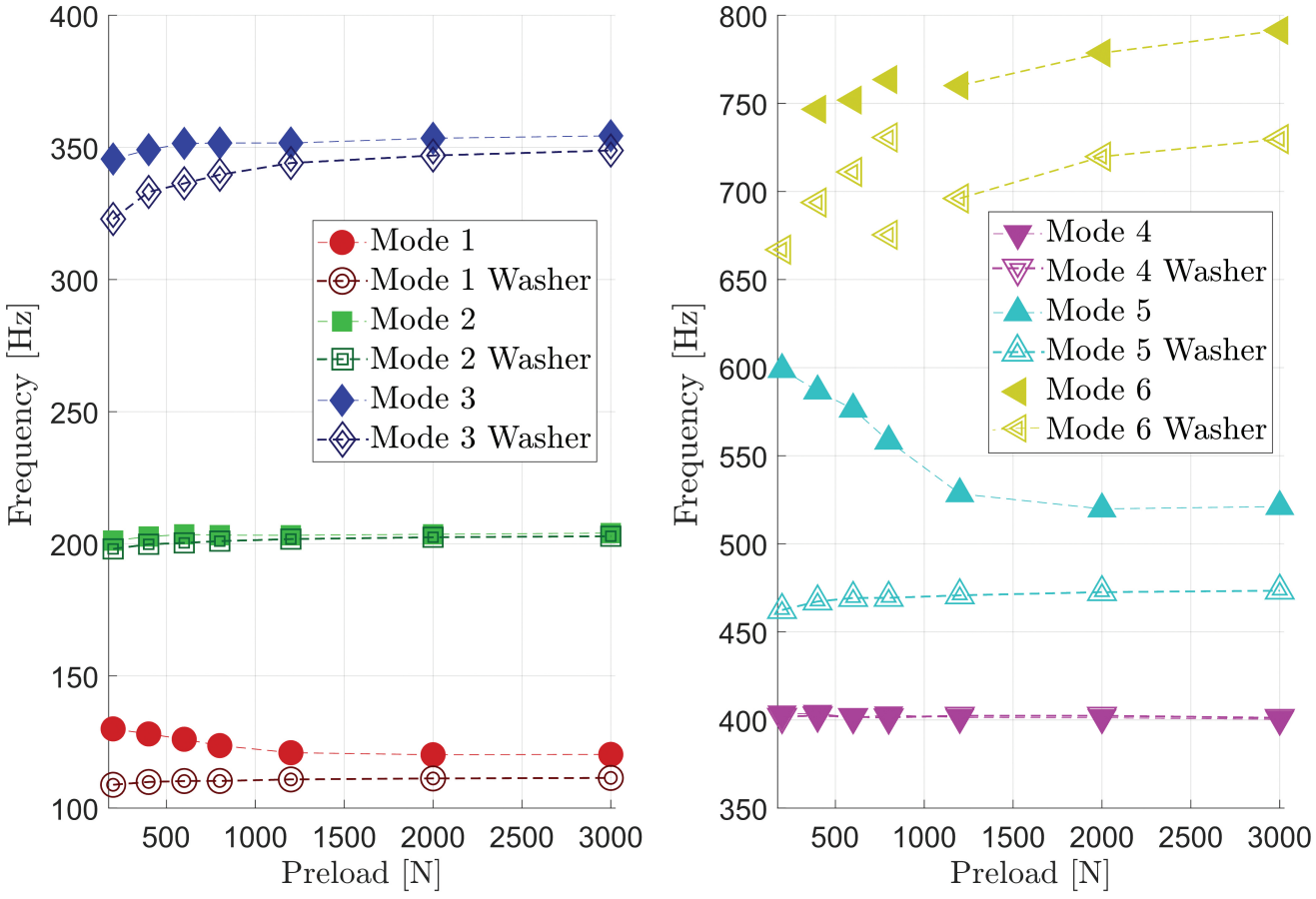

Fig. 16 Experimental mBARC natural frequencies for (left) modes 1–3 and (right) modes 4–6 vs. preload in bolts F1 and F2 with and without a washer added between the bridge and each blade

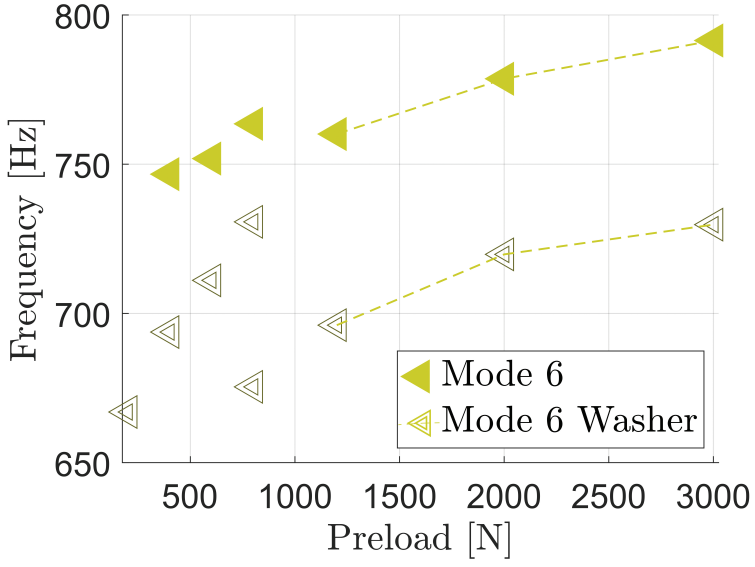

Fig. 17 Experimental mBARC mode 6 natural frequency vs. preload in bolts F1 and F2 with and without a washer added between the bridge and each blade. Below 1200 N there is low confidence in the mode 6 natural frequency due to the low amplitude of mode 6 in measured FRFs

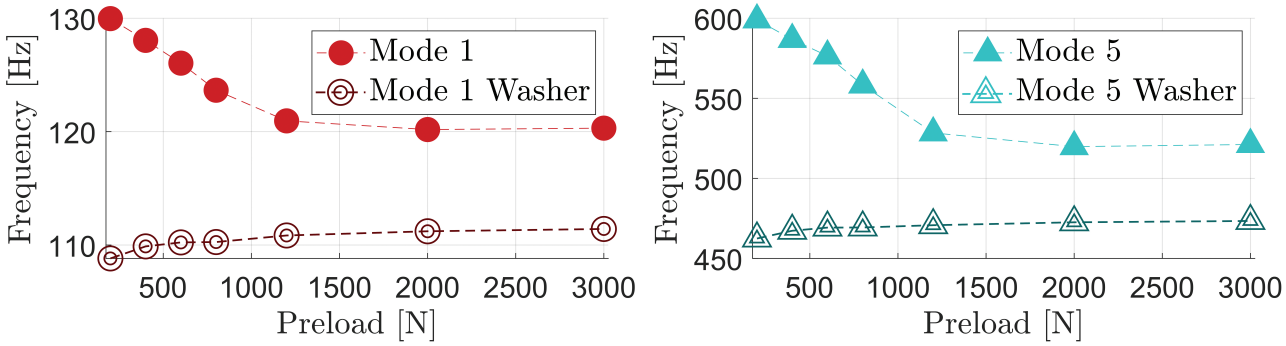

Fig. 18 Experimental mBARC natural frequencies for (left) mode 1 and (right) mode 5 vs. preload in bolts F1 and F2 with and without a washer added between the bridge and each blade. Fixing the contact area removes the decrease in natural frequency as preload increases

Shock Testing

For shock testing, high-energy impact excitation was applied to the mBARC at the location and in the direction shown in Fig. 3. An example measured shock response time series demonstrating a large decrease in the bolt F2 preload is shown is Fig. 19, though it should be noted this preload change was an outlier in the data; the average bolt F2 preload change was only -1.6 N. The filtered preload data shown in Fig. 19 was calculated by applying a zero-phase, third-order, low-pass Butterworth filter with a cutoff frequency of 20 Hz to the raw preload data (applied using the `filtfilt` function in MATLAB). For all shock excitation tests, the nominal initial preload of both the F1 and F2 bolts was 1000 N $\pm$ 20 N.

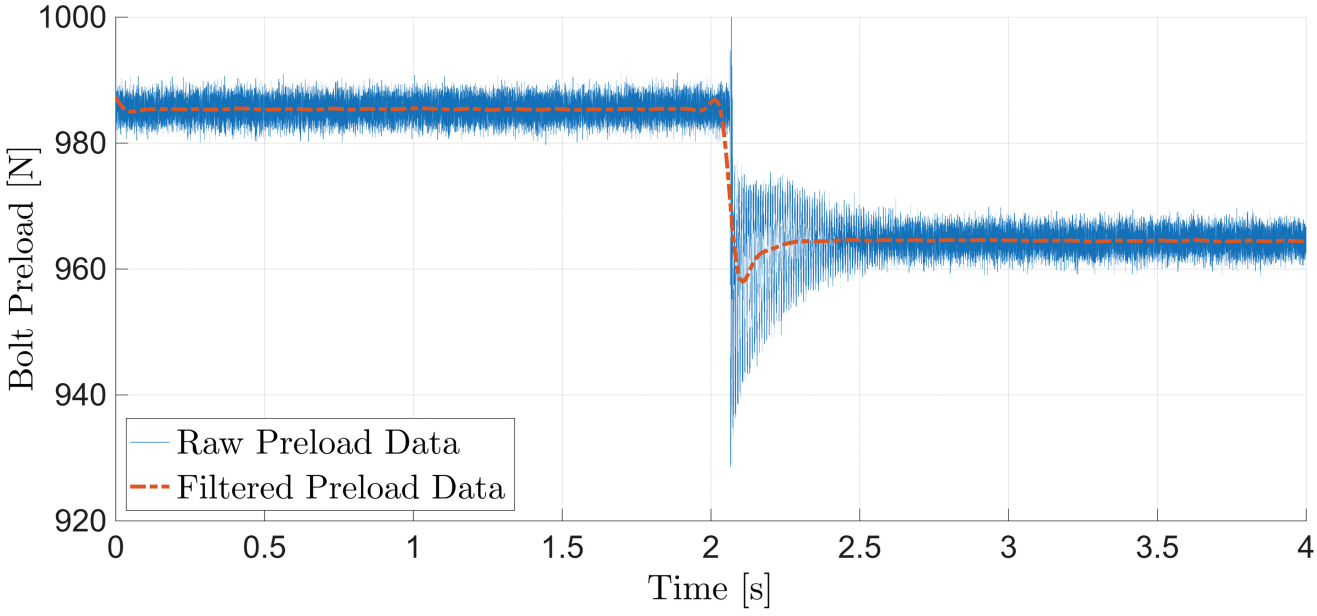

Fig. 19 Example measured shock response time series of bolt F2 preload. The shock excitation occurs just after 2 seconds, resulting in a rapid preload decrease between 2 and 2.5 seconds

As shown in Fig. 19, the preload remains stable before the shock and rapidly decreases immediately after the shock before settling at a lower preload. This preload drop shows the possibility of inducing bolt loosening for the mBARC. However, as stated previously, the extent of bolt loosening shown in Fig. 19 was an outlier. Figure 20 shows a histogram of the preload change over 36 different shocks. As shown in Fig. 20, loosening, tightening, and relatively no change among repeated bolt loosening trials was observed, with the mean and standard deviation of these trials shown in Table 2.

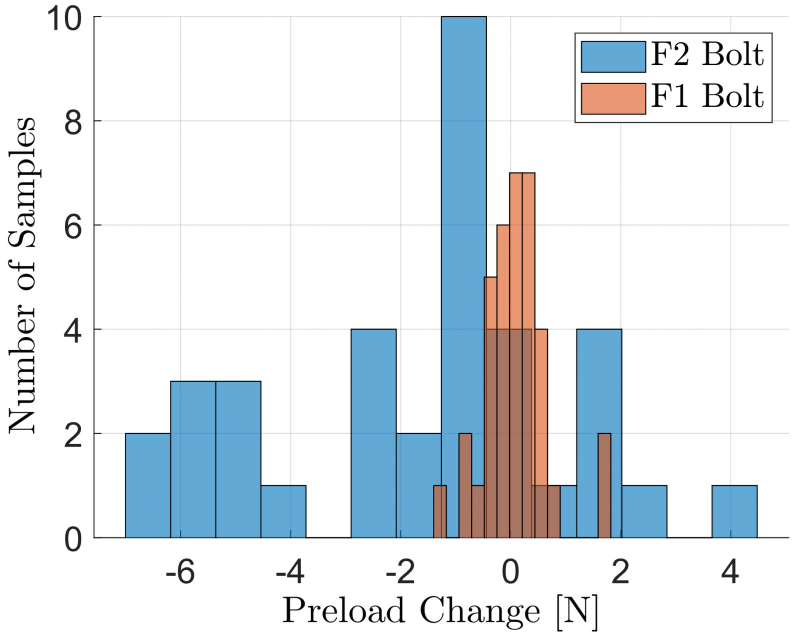

Fig. 20 Histogram of the preload change in bolts F1 and F2 resulting from 36 separate high-energy impact excitations. Bolt F2 experiences a larger range of preload change due to it being closer to the shock input location

Table 2 Mean and standard deviation of the preload change in bolts F1 and F2 for approximately 1000 N initial preload

	F1 [N]	F2 [N]
Mean Preload Change	0.098	−1.6
Standard Deviation	0.58	2.7

When applying shocks with peak magnitudes ranging from 200 N to 1100 N as was done here, no clear relationship was found between input force and change in preload. Though the results shown in Fig. 20 include a range of shock magnitudes, the preload change variation demonstrates that when the range of impact force is between 200 N and 1100 N and the initial bolt F1 and F2 preloads are both approximately 1000 N, the preload change of the as-manufactured mBARC is highly probabilistic and relatively small compared to the preload values themselves. Additionally, in [1] which considers three axially aligned rods and simulated shocks between 0 and 50 kN (i.e., regime 1 in [1]), the two joints act independently of each other. While the mBARC is a different structure than that in [1], the preload response of the mBARC has similar characteristics to regime 1 of the simulated axial rods in [1].

To track the change in mode frequencies in time during and after applying a shock excitation, the WT was used. For a linear system, mode natural frequencies do not change in time, and appear as horizontal bands in the WT whose amplitude decays depending on a given mode's damping and contribution to the measured response. For a nonstationary nonlinear system, however, the natural frequency, damping, and shape of a given mode can be time-dependent. Thus, for a structural system exhibiting nonstationary nonlinearities resulting from bolt loosening, the WT is an excellent tool for monitoring changes in natural frequencies in time, as was done in [13], for example.

Example WTs of a measured acceleration from the Z DOF of triaxial accelerometer 2 (see Fig. 7) considering a low-energy impact excitation (28.08 N peak force) from a modal test and a high-energy impact excitation (324.23 N peak force) from a shock test are shown in Fig. 21. In Fig. 21, the (largely) horizontal bands of the WT for the low-energy impact indicate a relatively linear response, with some minor nonlinearities seen primarily below 0.01 seconds. However, the more noticeable diagonal bands shown in the WT for the high-energy impact indicate a more significant nonlinear response. As demonstrated by the example WTs in Fig. 21 and from observations of WTs for other impact excitations, a key takeaway is that higher-energy impacts qualitatively appear to increase the nonlinearity in the system's shock response as expected. This result is similar to what is shown in [13], where a (relatively lower) 7 m/s impact velocity yielded a WT that only showed horizontal bands. However, for a (relatively higher) 13.5 m/s impact velocity, the WT showed non-horizontal bands for the first 0.05 seconds.

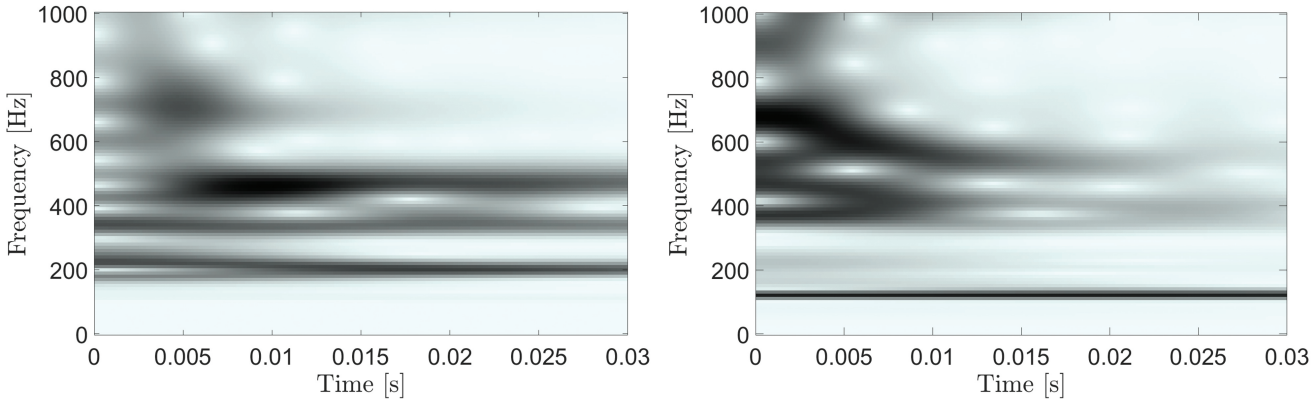

Fig. 21 Example WTs of a measured acceleration response considering (left) low-energy impact excitation and (right) high-energy impact excitation.

ROM Applicability

As discussed in the Contact Area Variability section, direct expansion and application of the ROM discussed in the Reduced-Order Model section to the as-manufactured mBARC was not achievable because of changes in the contact area between the bridge and blades resulting from varying the preloads of bolts F1 and F2. However, contact-area variation was mitigated by adding a washer between the bridge and each blade, which yielded more expected results (i.e., increasing natural frequencies with increasing preload) as shown in Fig. 16. While fixing the contact area more easily allows for the possibility of applying this ROM, expansion to include multiple nonlinear springs for bolts F1 and F2 may still be required depending on the shock excitation location and direction. In addition, modifications to a structure in this way may often not be permitted, and for the study here, significantly changed the mBARC as shown by the differences in natural frequencies with and without including these washers (see Figs. 16–18).

To further demonstrate the necessity of varying the contact area to capture mBARC bolt-loosening phenomena, additional parameter studies were conducted using the mBARC FEM to explore which parameters needed to be varied to match the modes of the FEM to experiment. Specifically, experimental modes which most significantly contributed to shock responses without washers between the blades and bridge (here, modes 1, 2, 3, and 5) were targeted, with other modes either not

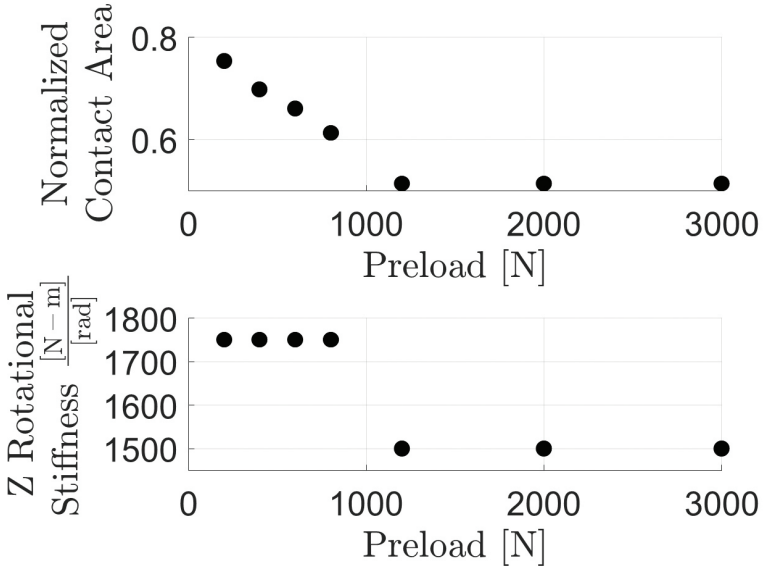

Fig. 22 (top) Normalized contact area and (bottom) Z rotational stiffness needed at each preload to match the natural frequencies of modes 1, 2, 3, and 5 of the mBARC FEM to experiment within 7% RMSE

being sensitive to the bushing element stiffness values and contact area (mode 4) or for which there was low confidence in the experimental natural frequencies (mode 6). This is similar to what is required for the ROM parameter identification, where FEM validation is needed at multiple preloads within a range of interest. Here, the normalized contact area and Z rotational stiffness were found to be the most influential parameters on the system's response. By varying these parameters alone, the natural frequencies of modes 1, 2, 3, and 5 of the mBARC FEM were able to be matched at each considered preload within 7% root mean squared error (RMSE). The final values of normalized contact area and Z rotational stiffness at each preload are shown in Fig. 22. Table 3 shows all other bushing element stiffness values when tuning the mBARC FEM, which were kept constant for all preloads. These results demonstrate that an expansion of the ROM to allow for contact area variation(s) in combination with stiffness variation(s) is needed to model mBARC bolt-loosening dynamics. More generally, this expansion is needed to apply this ROM for structures like the mBARC where the contact area of one or more bolted joints is required to be a function of preload to validate the FEM to experimental data.

Table 3 Constant bushing element stiffness values when tuning the mBARC FEM to match experimental natural frequencies at various preloads

Stiffness Direction	Value
X Axial [N/m]	10^7
Y Axial [N/m]	10^{10}
Z Axial [N/m]	10^8
X Rotational [N-m/rad]	10^8
Y Rotational [N-m/rad]	10^8

Conclusions

This research sought to extend the use and application of a previously developed ROM to capture bolt-loosening dynamics for a structure containing two bolted joints when considering a shock excitation. Here, the mBARC was considered, with the preload of the bolts connecting the blades and bridge varied to study the accelerations at points of interest to quantify bolt-loosening dynamics. After performing an initial validation of a BA-alone FEM to characterize the fixed-base BC, an mBARC FEM was developed and validated to match experimental natural frequencies within 7% RMSE for modes 1, 2, 3, and 5. Sensitivity studies were performed to study how different bushing element spring stiffness values and the contact area between the bridge and blades affected the natural frequencies of the mBARC FEM when attempting to match experimental values. Here, the contact area and Z rotational stiffness were found to be the most influential parameters. As part of mBARC FEM validation, the natural frequencies of the as-manufactured mBARC were measured with and without enforcing a constant contact area between the bridge and blades. This was done to study how changing contact area affects the natural frequencies of the first six system modes. The mBARC was also subjected to a range of high-energy shock excitations to characterize bolt loosening for this 2-bolt system. For impact excitations between 200 N and 1100 N, the bolt nearest to the shock loosened by an average of 1.6 N, though results were highly probabilistic. However, the bolt furthest from the shock excitation experienced relatively no change across all trials. The WT of measured accelerometer data was used to qualitatively demonstrate shock response dynamics for low- and high-energy impact excitations. High-energy impact excitations showed significantly more mode shifting, similar to results observed for structures studied in previous work. Lastly, with regard to applying and expanding the previously proposed ROM discussed in the Reduced-Order Model section, this ROM currently cannot model the preload change (and hence shock response dynamics) of the as-manufactured mBARC due to the contact area changing as a function of bolt preload. This was demonstrated both empirically with experimental modal testing and using a validated mBARC FEM where changing the contact area was necessary to match experimental natural frequencies at each preload.

Future Work

Based on the modeling and experimental results presented here, future research includes modifying the ROM in [13] to incorporate contact area variability as a function of preload. This would allow for the ROM to be applied to structures like the mBARC in which the contact area of one or more bolted joints is required to be a function of preload for FEM validation. In addition, efforts attempting to apply and expand this ROM to the mBARC with a fixed contact area between the bridge

and blades is of interest, as this may still yield insights into additional ROM modifications not discussed in this work. Lastly, increasing the number of bolts on the mBARC (or considering a nominal BARC structure) to study the dynamics of more complex bolted structures under shock excitation would be an interesting long-term future application of this research.

Acknowledgments This research was funded by Los Alamos National Laboratory (LANL) through the Engineering Institute's Los Alamos Dynamics Summer School (LADSS). The Engineering Institute is a research and education collaboration between LANL and the University of California San Diego's Jacobs School of Engineering. This collaboration seeks to promote multidisciplinary engineering in information research that develops and integrates advanced predictive modeling, novel sensing systems, and new developments in information technology to address LANL mission relevant problems. The authors would also like to acknowledge Alex Malliett of LANL for providing advice on sensors, data acquisition systems, and drilling additional holes into the BA to place the bridge for mBARC assembly, Fabian Vigil, Nathanael Adler, Steve Simmonds, and Roman Romero of LANL for help in wiring the load washers used for experimental efforts, Kai Newhouse of LANL and Dr. Jim Declerck of Michigan Technological University for help setting up and using Siemens Testlab, Jason Martinez, Cindy Lopez, and Amy Schiffer of LANL for administrative support of the Engineering Institute and assistance during the course of this work, and Dr. Samantha Ceballes and Dr. Shannon Danforth of LANL for leading the 2025 LADSS program.

References

1. Sandro Aldana and Keegan J Moore. Dynamic interactions between two axially aligned threaded joints undergoing loosening. *Journal of Sound and Vibration*, 520:116625, 2022. https://doi.org/10.1016/j.jsv.2021.116625
2. Guo-Ping Luo, Liang-Jun Xu, and Ji-Gao Zhang. Combination effect of fretting and corrosion on bolt-type power connectors. In *Electrical Contacts - 2000. Proceedings of the Forty-Sixth IEEE Holm Conference on Electrical Contacts (Cat. No.00CB37081)*, pages 60–66, 2000. https://doi.org/10.1109/HOLM.2000.889912
3. Long Yang, Bing Yang, Guangwu Yang, Yang Xu, Shoune Xiao, Shilin Jiang, and Jingsong Chen. Analysis of competitive failure life of bolt loosening and fatigue. *Engineering Failure Analysis*, 129:105697, 2021. https://doi.org/10.1016/j.engfailanal.2021.105697
4. Kai Jiang, Zhifeng Liu, Tao Zhang, and Feng Wang. Influence of bolt creep induced pre-tightening force relaxation on dynamic response of the bolted joint system. *Journal of Sound and Vibration*, 596:118800, 2025. https://doi.org/10.1016/j.jsv.2024.118800
5. Long Yang, Bing Yang, Guangwu Yang, Shoune Xiao, and Shilin Jiang. Research on factors affecting competitive failure between loosening and fatigue of bolt under combined excitation. *Journal of Constructional Steel Research*, 189:107110, 2022. https://doi.org/10.1016/j.jcsr.2021.107110
6. Gerhard H. Junker. New Criteria for Self-Loosening of Fasteners Under Vibration. *SAE Transactions*, 78:314–335, 1969. https://doi.org/10.4271/690055
7. N.G. PAI and D.P. HESS. Experimental study of loosening of threaded fasteners due to dynamic shear loads. *Journal of Sound and Vibration*, 253(3):585–602, 2002. https://doi.org/10.1006/jsvi.2001.4006
8. Matthew S. Allen, Daniel Rixen, Maarten van der Seijs, Paolo Tiso, Thomas Abrahamsson, and Randall L. Mayes. *Model Reduction Concepts and Substructuring Approaches for Linear Systems*, pages 25–73. Springer International Publishing, Cham, 2020. https://doi.org/10.1007/978-3-030-25532-9_3
9. Valentin Fort, Abdel-Hakim Bouzid, and Michel Gratton. Analytical Modeling of Self-Loosening of Bolted Joints Subjected to Transverse Loading. *Journal of Pressure Vessel Technology*, 141(3):031205, 03 2019. https://doi.org/10.1115/1.4042798
10. Toshimichi Fukuoka and Masataka Nomura. Proposition of Helical Thread Modeling With Accurate Geometry and Finite Element Analysis. *Journal of Pressure Vessel Technology*, 130(1):011204, 01 2008. https://doi.org/10.1115/1.2826433
11. Mingyuan Zhang, Dongfang Zeng, Liantao Lu, Yuanbin Zhang, Jing Wang, and Jingmang Xu. Finite element modelling and experimental validation of bolt loosening due to thread wear under transverse cyclic loading. *Engineering Failure Analysis*, 104:341–353, 2019. https://doi.org/10.1016/j.engfailanal.2019.05.001
12. Shriram Dravid. Study of vibration loosening of bolted joints–A review, *IAETSD Journal for Advanced Research in Applied Sciences*, 2018.
13. Keegan J Moore. A Reduced-Order Model for Loosening of Bolted Joints Subjected to Axial Shock Excitation. *Journal of Applied Mechanics*, 86(12):121007, 2019. https://doi.org/10.1115/1.4044813
14. Mingpo Zheng, Wentao Chen, Xing Yan, Zhifeng Liu, and Magd Abdel Wahab. Finite element analysis of bolted joints under torsional loads. *Tribology International*, 201:110188, 2025. https://doi.org/10.1016/j.triboint.2024.110188
15. Robert C. Juvinall and Kurt M. Marshek. *Fundamentals of Machine Component Design*, Chapter 10: Threaded Fasteners and Power Screws, page 430. John Wiley & Sons Inc., 2000.
16. Felipe Camargo de Oliveira Kobayashi, Blake Johnson, Aryan Singh, and Keegan J. Moore. A mathematical approach to representing nonlinear dynamics of bolted joint loosening, 2024.
17. Kyle Brindley, Prabhu Khalsa, Thomas Roberts, Sergio Cordova, Matthew Fister, Chris Johnson, and Scott Ouellette. waves, June 2025. https://doi.org/10.5281/zenodo.7574167